THE JOURNAL OF BIOLOGICAL CHEMISTRY VOL. 287, NO. 30, pp. 25241–25254, July 20, 2012

Discovery of a Novel Allosteric Modulator of 5-HT_3 Receptors

*INHIBITION AND POTENTIATION OF CYS-LOOP RECEPTOR SIGNALING THROUGH A CONSERVED TRANSMEMBRANE INTERSUBUNIT SITE**

Received for publication, March 8, 2012, and in revised form, May 11, 2012 Published, JBC Papers in Press, May 15, 2012, DOI 10.1074/jbc.M112.360370

Sarah M. Trattnig[‡1], Kasper Harpsøe[‡1], Sarah B. Thygesen[‡], Louise M. Rahr[‡], Philip K. Ahring[§], Thomas Balle[‡], and Anders A. Jensen[‡2]

From the [‡]Department of Drug Design and Pharmacology, Faculty of Health and Medical Sciences, University of Copenhagen, Universitetsparken 2, DK-2100 Copenhagen, Denmark and [§]NeuroSearch A/S, Pederstrupvej 93, DK-2750 Ballerup, Denmark

Background: The 5-HT_3 receptors belong to the Cys-loop receptor superfamily.
Results: The novel 5-HT_3 antagonist PU02 (6-[(1-naphthylmethyl)thio]-*9H*-purine) is discovered, and its mechanism of action is delineated.
Conclusion: PU02 is a potent and selective negative allosteric modulator of 5-HT_3 receptors acting through a transmembrane intersubunit site in the receptors.
Significance: The study highlights the transmembrane subunit interface in the Cys-loop receptor as a hot spot for allosteric modulation.

The ligand-gated ion channels in the Cys-loop receptor superfamily mediate the effects of neurotransmitters acetylcholine, serotonin, GABA, and glycine. Cys-loop receptor signaling is susceptible to modulation by ligands acting through numerous allosteric sites. Here we report the discovery of a novel class of negative allosteric modulators of the 5-HT_3 receptors (5-HT_3Rs). PU02 (6-[(1-naphthylmethyl)thio]-*9H*-purine) is a potent and selective antagonist displaying IC_{50} values of ~1 μM at 5-HT_3Rs and substantially lower activities at other Cys-loop receptors. In an elaborate mutagenesis study of the 5-HT_3A receptor guided by a homology model, PU02 is demonstrated to act through a transmembrane intersubunit site situated in the upper three helical turns of TM2 and TM3 in the (+)-subunit and TM1 and TM2 in the (−)-subunit. The Ser^{248}, Leu^{288}, Ile^{290}, Thr^{294}, and Gly^{306} residues are identified as important molecular determinants of PU02 activity with minor contributions from Ser^{292} and Val^{310}, and we propose that the naphthalene group of PU02 docks into the hydrophobic cavity formed by these. Interestingly, specific mutations of Ser^{248}, Thr^{294}, and Gly^{306} convert PU02 into a complex modulator, potentiating and inhibiting 5-HT-evoked signaling through these mutants at low and high concentrations, respectively. The PU02 binding site in the 5-HT_3R corresponds to allosteric sites in anionic Cys-loop receptors, which emphasizes the uniform nature of the molecular events underlying signaling through the receptors. Moreover, the dramatic changes in the functional properties of PU02 induced by subtle changes in its binding site bear witness to the delicate structural discrimination between allosteric inhibition and potentiation of Cys-loop receptors.

The 5-hydroxytryptamine type 3 receptors (5-HT_3Rs)[3] are pentameric ligand-gated cation-selective ion channels belonging to the Cys-loop receptor superfamily, which also contains nicotinic acetylcholine receptors (nAChRs), γ-aminobutyric acid type A receptors ($GABA_A$Rs), and glycine receptors (GlyRs) (1–6). The receptors are homomeric or heteromeric complexes, and the existence of numerous subunits gives rise to a plethora of physiologically relevant subtypes. The human 5-HT_3R family contains the five subunits 5-HT3A to -E, which form homomeric 5-HT_3A and heteromeric 5-HT_3AB, 5-HT_3AC, 5-HT_3AD and 5-HT_3AE receptors (1–3). The 5-HT_3Rs mediate numerous important functions in serotonergic neurotransmission and as heteroreceptors in other neurotransmitter systems (1). Thus, the receptors are pursued as drug targets in various psychiatric disorders, and 5-HT_3R antagonists are used to treat postoperative nausea and nausea/emesis connected with chemotherapy and radiotherapy (1).

The Cys-loop receptor is composed of three structural entities: an extracellular domain (ECD) made up by the N-terminal domains, a transmembrane domain (TMD) composed of the four transmembrane α-helices TM1 to -4, and an intracellular domain formed by the second intracellular loops in the five subunits in the complex. Considerable insight into the three-dimensional architecture of Cys-loop receptors has emerged from electron microscopy images of the *Torpedo* nAChR (7) and from high resolution x-ray structures of ACh-binding pro-

* This work was supported by grants from the Lundbeck Foundation (to S. M. T., T. B., and A. A. J.), the Carlsberg Foundation (to K. H. and A. A. J.), the Drug Research Academy, FARMA, University of Copenhagen (to K. H. and T. B.), the Danish Medical Research Council (to A. A. J.), and the Novo Nordisk Foundation (to A. A. J.). Part of this work was presented in the form of a poster by S. M. T. at the Society of Neuroscience conference in San Diego, November 13–17, 2010.
[1] Both authors are co-first authors.
[2] To whom correspondence should be addressed: Dept. of Drug Design and Pharmacology, Faculty of Health and Medical Sciences, University of Copenhagen, Universitetsparken 2, DK-2100 Copenhagen, Denmark. Tel.: 45-39179650; Fax: 45-35336041; E-mail: aaj@farma.ku.dk.

[3] The abbreviations used are: 5-HT_3R, 5-hydroxytryptamine type 3 receptor; 5-HT, 5-hydroxytryptamine; ECD, extracellular domain; FMP, FLIPR™ Membrane Potential Blue; $GABA_A$R, γ-aminobutyric acid type A receptor; GlyR, glycine receptor; HEK293, human embryonic kidney 293; NAM, negative allosteric modulator; nAChR, nicotinic acetylcholine receptor; ACh, acetylcholine; PAM, positive allosteric modulator; TMD, transmembrane domain; ELIC, *E. chrysanthemi* pentameric ligand-gated ion channel.

teins (8) and of prokaryotic (9–12) and invertebrate (13) Cys-loop receptor orthologs. These structures and biochemical, biophysical and mutagenesis studies performed over the years have also shed light on the allosteric transitions underlying receptor signal transduction. The signaling is initiated by agonist binding to the orthosteric sites situated at subunit interfaces in the ECD, which subsequently triggers a number of allosteric events leading to the opening of the ion channel in the TMD (5, 14–16).

The allosteric nature of the Cys-loop receptor complex implies that the signal elicited by orthosteric agonists can be modulated by ligands binding to other receptor regions (5, 14–16). Numerous positive and negative allosteric modulators (PAMs and NAMs, respectively) of Cys-loop receptors have been identified, and new generations of allosteric modulators of GABA$_A$Rs and nAChRs comprise several potent and selective drugs and highly interesting pharmacological tools (5, 6, 16–18). In contrast, the allosteric modulators of 5-HT$_3$Rs reported to date, including *n*-alcohols, volatile and intravenous anesthetics, and various antidepressants and antipsychotics, are all characterized by promiscuous pharmacological profiles and by displaying low potencies at the 5-HT$_3$Rs (19).

In the present study, the pharmacological properties and mechanism of action of a novel 5-HT$_3$R NAM, PU02, are characterized, and its transmembrane intersubunit binding site in the 5-HT$_3$A receptor is identified and mapped. Interestingly, several mutations in this site convert PU02 into a complex modulator with a biphasic PAM/NAM profile, which underlines the intricate linkage between the site and channel gating in the 5-HT$_3$R.

EXPERIMENTAL PROCEDURES

Materials—Culture media, serum, antibiotics, and buffers for cell culture were obtained from Invitrogen. The compound library and PU01 analogs were obtained from Chembridge Corp. (San Diego, CA). Glycine, GABA, ACh, serotonin, and probenecid were purchased from Sigma, and ondansetron, granisetron, tropisetron, genistein, and epibatidine were obtained from Tocris Cookson (Bristol, UK). The FLIPR^{TM} Membrane Potential Blue (FMP) assay and Fluo-4/AM dyes were purchased from Molecular Devices (Crawley, UK) and Molecular Probes, Inc. (Eugene, OR), respectively. [^{3}H]GR65630 and Opti-Fluor^{TM} were obtained from Perkin-Elmer Life Sciences. The cDNAs encoding for the human 5-HT3A and 5-HT3B subunits were kind gifts from Drs. J. Egebjerg and E. F. Kirkness, respectively, and cDNAs for the human α1, β2, and γ2s GABA$_A$R subunits were kindly provided by Dr. P. J. Whiting. The stable h5-HT$_3$A-HEK293 cell line used for the FMP assay experiments was a kind gift from Dr. J. Egebjerg, and the stable h5-HT$_3$A- and h5-HT$_3$AB-HEK293 cell lines used in the Ca^{2+}/Fluo-4 assay were kind gifts from Dr. C. Rojas (20). The stable cell lines expressing rat α3β4, mouse α4β2, and human α7 nAChRs were kind gifts from Drs. Y. Xiao and K. J. Kellar, J. A. Stitzel, and D. Feuerbach, respectively (21–23). The construction and pharmacological characterization of the stable HEK293 cell lines expressing the human α1 GlyR and human ρ1 GABA$_A$R have been described previously (24, 25).

Molecular Biology—The generation of 5-HT3A-pCIneo and 5-HT3B-pCIneo plasmids has been described previously (26, 27). Human 5-HT3C and 5-HT3E cDNAs were cloned by PCR from I.M.A.G.E. clones (Source BioScience, Nottingham, UK) and subcloned into pCDNA3.1 using the restriction enzymes NheI/ApaI and NheI/XhoI, respectively. Mutations were introduced into 5-HT3A-pCIneo using the QuikChange mutagenesis kit (Stratagene). All generated cDNAs were verified by sequencing.

Cell Culture and Transfections—All cell lines were cultured in a humidified atmosphere of 5% CO_2 and 95% air at 37 °C. The mα4β2-HEK293, hα7-GH3, rα3β4-HEK293, and h5-HT$_3$A-HEK293 cells (from Dr. Egebjerg) were grown in Dulbecco's modified Eagle's medium (DMEM) supplemented with penicillin (100 units/ml), streptomycin (100 μg/ml), 10% fetal bovine serum, 0.1 mg/ml zeocin, and either 0.5 mg/ml hygromycin (mα4β2), 0.1 mg/ml G-418 (hα7), or 1 mg/ml G-418 (rα3β4 and h5-HT$_3$A). The h5-HT$_3$A- and h5-HT$_3$AB-HEK293 cell lines (from Dr. Rojas) were grown in RPMI 1640 containing penicillin (100 units/ml), streptomycin (100 μg/ml), and 10% fetal bovine serum and supplemented with 0.5 mg/ml G-418 (h5-HT$_3$A) or 0.5 mg/ml G-418 and 3 μg/ml blasticidin (h5-HT$_3$AB).

The tsA201 cells were grown in DMEM supplemented with penicillin (100 units/ml), streptomycin (100 μg/ml), and 10% fetal bovine serum. At the day of transfection, 8×10^5 tsA201 cells were split into a 6-cm tissue culture plate and transfected the following day with a total of 4 μg of cDNA using PolyFect transfection reagent according to the manufacturer's instructions (Qiagen, Hilden, Germany). Thus, the cells were transfected with 4 μg of WT or mutant 5-HT3A-pCI-neo (generating homomeric 5-HT$_3$A receptors) or with 1 μg of 5-HT3A-pCI-neo together with 3 μg of 5-HT3B-pCI-neo, 3 μg of 5-HT3C-pCDNA3.1/Hygro(+), or 3 μg of 5-HT3E-pCDNA3.1/Hygro(+) (giving rise to heteromeric 5-HT$_3$AB, 5-HT$_3$AC, and 5-HT$_3$AE receptors, respectively). The cells were assayed 36–48 h after the transfection.

COS-7 cells were cultured in DMEM supplemented with 10% (v/v) fetal bovine serum and were transiently transfected with WT or mutant 5-HT3A-pCIneo together with a plasmid encoding for green fluorescent protein using the Lipofectamine Plus transfection kit as described by the manufacturer (Invitrogen). Cells were used 48–72 h after transfection.

FMP Assay—The screening of the compound library at the h5-HT$_3$A-HEK293 cell line and the subsequent functional characterization of the compounds were performed in the FMP assay essentially as described previously (28). Stable h5-HT$_3$A-, mα4β2-, rα3β4-, hα1-, and hρ1-HEK293 cell lines or tsA201 cells transiently transfected with 5-HT$_3$Rs or α1β2γ2s GABA$_A$R were split into poly-D-lysine-coated black 96-well plates with clear bottoms (BD Biosciences). 16–24 h later, the medium was aspirated, and the cells were washed with 100 μl of Krebs buffer (140 mM NaCl, 4.7 mM KCl, 2.5 mM $CaCl_2$, 1.2 mM $MgCl_2$, 11 mM HEPES, 10 mM D-glucose, pH 7.4). 50 μl of Krebs buffer was added to the wells (in the antagonist experiments, various concentrations of the antagonist were dissolved in the buffer), and then an additional 50 μl of Krebs buffer supplemented with the FMP assay dye (1 mg/ml) was added to each

well. Then the plate was incubated at 37 °C in a humidified 5% CO_2 incubator for 30 min and assayed in a NOVOstar^{TM} plate reader (BMG Labtechnologies, Offenburg, Germany) measuring emission (in fluorescence units) at 560 nm caused by excitation at 530 nm before and up to 1 min after the addition of 33 μl of agonist solution. The experiments were performed in duplicate at least three times for each compound at each WT and mutant receptor. EC_{70}–EC_{90} concentrations of serotonin, epibatidine, glycine, and GABA were used as agonist concentrations for the antagonist experiments at the respective 5-HT$_3$Rs, nAChRs, GlyRs, and GABA$_A$Rs. In the preincubation experiments (Fig. 4*C*), cells were incubated with Krebs buffer or with Krebs buffer supplemented with 30 μM PU02 or 10 nM ondansetron for 30 min followed by three washes with Krebs buffer before execution of the assay.

Ca^{2+}/Fluo-4 Assay—The functional characterization of compounds at the hα7-GH3 cell line and at the h5-HT$_3$A and h5-HT$_3$AB cell lines (from Dr. C. Rojas) was performed in the Ca^{2+}/Fluo-4 assay essentially as described previously (28). Cell lines were split into poly-D-lysine-coated black 96-well plates with clear bottoms. Following a 16–24-h incubation in the case of the 5-HT$_3$R cell lines or a 64–72-h incubation of the hα7-GH3 cells, the culture medium was aspirated, and the cells were incubated in 50 μl of assay buffer (Hanks' buffered saline solution containing 20 mM HEPES, 1 mM $CaCl_2$, 1 mM $MgCl_2$, and 2.5 mM probenecid, pH 7.4) supplemented with 6 mM Fluo-4/AM at 37 °C for 1 h. Then the buffer was aspirated, the cells were washed once with 100 μl of assay buffer, and then 100 μl of assay buffer was added to the cells. The assay buffer used for the hα7-GH3 cells was supplemented with 100 μM genistein. The 96-well plate was assayed in a NOVOstar^{TM} microplate reader measuring emission (in fluorescence units) at 520 nm caused by excitation at 485 nm before and up to 60 s after the addition of 33 μl of agonist solution in assay buffer. Serotonin was used as agonist for the h5-HT$_3$A and h5-HT$_3$AB receptors, whereas ACh was used for the α7 nAChR.

[^{3}H]GR65630 Binding—The [^{3}H]GR65630 competition binding assay was performed as described previously using membranes from stable h5-HT3A-HEK293 cells (29). Briefly, cells were harvested at 80–90% confluence and scraped into the assay buffer (Hanks' buffered saline solution containing 20 mM HEPES, 1 mM $CaCl_2$, 1 mM $MgCl_2$, and 2.5 mM probenecid, pH 7.4), homogenized using a Polytron homogenizer for 10 s, and centrifuged for 20 min at 50,000 × *g*. The resulting pellet was homogenized in 30 ml of assay buffer and centrifuged again. Then the cell pellet was resuspended in the assay buffer, and the membranes were incubated with 50 pM [^{3}H]GR65630 and various concentrations of the test compounds in a total reaction volume of 800 ml under gentle shaking for 1 h at room temperature. The incubation was terminated by a rapid filtration through Whatman GF/C filters (Whatman, Maidstone, UK) presoaked for 30 min in 0.3% (w/v) polyethyleneimine, followed by three washes with 3 ml of ice-cold isotonic saline solution. Filters were then transferred into vials containing 3 ml of Opti-Fluor scintillation solution, and radioactivity was measured in a liquid scintillation counter. The experiments were performed in duplicate a total of three times. The level of total binding was <10% of free radioligand for all samples.

Electrophysiology—COS-7 cells expressing the WT or mutant 5-HT$_3$A receptors were recorded in the whole cell voltage clamp configuration (30) at room temperature. Cells were superfused with extracellular solution (140 mM NaCl, 11 mM glucose, 10 mM HEPES, 4.7 mM KCl, 0.1 mM $CaCl_2$, adjusted to pH 7.4 with NaOH), patch pipettes had a resistance of ~2 megaohms when filled with intracellular solution (120 mM KCl, 1.8 mM $MgCl_2$, 10 mM EGTA, 10 mM HEPES, adjusted to pH 7.4 with KOH), and recordings were performed as described previously (31).

All data were obtained with an EPC-9 amplifier (HEKA Electronics, Lambrect, Germany) run by a Windows XP personal computer. Experimental conditions and data acquisition were set and obtained using the PULSE software accompanying the amplifier. Data were low pass-filtered and sampled directly to the hard disk, and cells were held at −60 mV during recordings. Pipettes were pulled from borosilicate glass using a horizontal electrode puller (Zeitz Instrumente, Augsburg, Germany). The cells were rinsed with phosphate-buffered saline and detached from the culture flask by tripleX (0.1% (w/v)) digestion for 2 min at 37 °C and seeded on the day of the experiment. Glass coverslips (3.5 mm) precoated with poly-D-lysine (0.005% (w/v)) were placed in Petri dishes, and cells were added at a suitable density.

Coverslips with cultured cells were transferred to a perfusion chamber mounted on the stage of an inverted microscope supplied with Nomarski optics, where transfected cells were identified by green fluorescence. Compounds were dissolved in extracellular solution and applied to the patched cell through a double-barreled application pipette. Application pipettes were fabricated from θ glass tubes (1.5 mm outer diameter; WPI, Sarasota, FL) and mounted on a piezoelectric device (PZS-100HS; Burleigh Instruments, Quebec, Canada) connected to a piezo-driver (PZ-150M, Burleigh Instruments) driven by TTL pulses from the EPC-9 amplifier. Approximately 1 min after the onset of the gravity flow, a PULSE protocol was initiated, and the current was recorded in 45-s intervals until peak amplitudes were stable. For transfected COS-7 cells, the duration of the recording periods was 6 s, during which the application pipette was switched to the agonist-containing test solution for 500 ms.

Data Analysis—All analysis and curve fitting were performed using Prism (version 5.0d; GraphPad Software, San Diego, CA). Concentration-response curves for agonists and concentration-inhibition curves for antagonists obtained in the FMP and Ca^{2+}/Fluo-4 assays were constructed based on the difference in the fluorescence units between the maximal fluorescence recording made before and after the addition of agonist obtained for different concentrations of the respective ligands.

Concentration-response data for 5-HT were fitted to a sigmoidal curve with variable slope using nonlinear regression,

$$Y = \text{bottom} + (\text{top} - \text{bottom})/(1 + (10^{(\log EC_{50} - X)} \times n_H)) \quad \text{(Eq. 1)}$$

where X represents the logarithm of the 5-HT concentration, Y is the response, and n_H is the Hill slope.

Concentration-inhibition data for the antagonists were fitted to a sigmoidal curve with variable slope using nonlinear regression,

$$Y = \text{bottom} + (\text{top} - \text{bottom})/(1 + 10^{(\log IC_{50} - X)} \times n_H) \quad \text{(Eq. 2)}$$

where X represents the logarithm of the antagonist concentration, Y is the response, and n_H is the Hill slope.

The EC_{50} values for 5-HT and IC_{50} values for the antagonists were derived from these equations. The maximal responses (R_{max} values) elicited by 5-HT through the various mutants were derived from the fitted concentration-response curves, and the values were normalized to the R_{max} value obtained for 5-HT at cells expressing the WT receptor on the same plate.

Statistical analysis of pIC_{50} and pEC_{50} values obtained in the mutagenesis study was performed for mean ± S.E. values in GraphPad Instat (San Diego, CA) by one-way analysis of variance followed by Dunnett's multiple comparisons test ($p > 0.05$), using the data for the WT 5-HT$_3$A receptor as control.

As for the electrophysiological data, concentration-response data for each cell were normalized to the maximum current for that cell. 5-HT-induced macroscopic currents were extracted from PULSE (HEKA, Lamprecht, Germany) and subsequently analyzed using IgorPro (Wavemetrics, Lake Oswego, OR) software. All electrophysiology data are based on recordings at more than four different cells on different days and transfections.

Determination of Time Constants for the Association and Desensitization Phases of 5-HT Currents—Relevant sections of the rising phase (for association) of selected traces were fitted to the single exponential equation, $f(x) = y_{max} \times (1 - \exp(-x/\tau))$, and sections in the decay phase (for desensitization) of representative traces were fitted to the single exponential equation, $f(x) = (y_{max} - \text{bottom}) \times \exp(-x/\tau) + \text{bottom}$, using IgorPro. Time constant values for WT and mutant receptors obtained in the absence or presence of PU02 were compared for significant difference using paired Student's t test statistical analysis in Prism (95% confidence interval). Time constant values for WT and mutant receptors were compared with each other using one-way analysis of variance in conjunction with Dunnett's multiple comparisons test in Prism.

Amino Acid Sequence Alignments—The coordinates and sequences of the *Erwinia chrysanthemi* pentameric ligand-gated ion channel (ELIC) crystal structure, Protein Data Bank code 2VL0 (9), and the NMR structure of the transmembrane domain of human nAChR β2 subunit, Protein Data Bank code 2KSR (32), were downloaded from the Protein Data Bank (33). Initially, we aligned the sequences of ELIC and β2 using version 8.99 of T-Coffee (34). Next, we imported the first conformer of the β2 structure and the structure of ELIC into PyMOL (35) and overlaid them by superimposing the backbone atoms of those residues in TM1 and TM2, which were identical or highly similar in the T-Coffee alignment. This superimposition was used to anchor the alignment of TM3 on Ile^{106} and Val^{107} in β2 plus Ile^{276} and Leu^{277} in ELIC to obtain a structurally based alignment of TM1 to -3 in the two structures.

The sequences of human 5-HT3A, β2 nAChR, and α1 and β3 $GABA_A$ subunits were retrieved from the Protein Knowledgebase (36) (entries P46098, P17787, P14867, and P28472, respectively) along with the sequences of all other human nAChRs, 5-HT$_3$Rs, GlyRs, and $GABA_A$Rs. A sequence alignment of all human Cys-loop receptors was then created using version 8.99 of T-Coffee (34), and we extracted the 5-HT3A, β2 nAChR, and α1 and β3 $GABA_A$R sequences of TM1 to -3, as defined by the helices in the β2 nAChR NMR structure. The ELIC sequence of TM1 to -3 was added to this alignment by use of the β2 nAChR sequence and the structurally derived alignment described above. The resulting alignment is in agreement with a very recently published alignment including some of the same sequences (13) but which is not based on the β2 nAChR NMR structure.

Homology Modeling—A homology model of a dimer interface consisting of TM1 to -3 in h5-HT$_3$A was constructed using version 9.9 of Modeller (37) with TM1 to -3 from chain A and B of the ELIC crystal structure as a template and the amino acid sequence alignment of 5-HT3A and ELIC described above. N- and C-terminal ends of the helices were capped with the ACE and CT3 capping groups, respectively, and helical constraints were added to those parts of 5-HT3A where the β2 nAChR NMR structure shows a helical structure, whereas ELIC does not: the C-terminal end of TM1 (residues 261–265) and the N- and C-terminal ends of TM3 (residues 303–307 and 325–329). A total of 100 models were constructed using the fastest optimization protocol, and the best scoring model was selected based on the built-in DOPE (discrete optimized protein energy) homology model scoring function (38).

RESULTS

Discovery of a Novel Class of 5-HT$_3$R Antagonists—A screening of a commercial library consisting of 1,680 compounds at a human 5-HT$_3$A-HEK293 cell line using the FMP assay identified PU01 (2-amino-6-[(1-naphthylmethyl)thio]-*9H*-purine) as an antagonist of the receptor (Fig. 1). The structure-activity relationship of this scaffold was elucidated by functional characterization of PU01 and 27 analogs at the receptor. Eight compounds in the series antagonized 5-HT$_3$A receptor signaling in a concentration-dependent manner (IC_{50} values of 0.49–12 μM), whereas the rest of the analogs were inactive or displayed negligible antagonist activity at the receptor (Fig. 1). The PU02 analog (6-[(1-naphthylmethyl)thio]-*9H*-purine) (Fig. 2*A*) was selected for the subsequent studies.

Selectivity profile of PU02—PU02 displayed similar IC_{50} values as an antagonist at the human 5-HT$_3$A, 5-HT$_3$AB, 5-HT$_3$AC, and 5-HT$_3$AE receptor subtypes expressed in tsA201 cells in the FMP assay (Table 1). This profile was verified in a Ca^{2+}/Fluo-4 assay, where PU02 inhibited both 5-HT$_3$A and 5-HT$_3$AB receptor signaling with high nanomolar IC_{50} values (Fig. 2*A*). PU02 also inhibited α7 and α3β4 nAChR signaling but with IC_{50} values 10–30 and 30–100 fold higher, respectively, than those at the 5-HT$_3$Rs (Fig. 2*B* and Table 1). PU02 was inactive when tested as agonist, potentiator, and antagonist at the α4β2 nAChR, at the α1 GlyR, and at ρ1 and α1β2γ2s $GABA_A$Rs (Table 1).

Electrophysiological Characterization of PU02—The functional characteristics of PU02 at 5-HT$_3$A expressed in COS-7 cells were determined by the whole cell patch clamp technique. In agreement with previous studies (26, 39), 5-HT elicited currents through the 5-HT$_3$A receptor with an EC_{50} of 8.1 μM (pEC_{50} ± S.E. = 5.10 ± 0.08) and a Hill slope of 1.13 ± 0.27 (n = 6). PU02 inhibited the signal elicited by 20 μM 5-HT ($\sim EC_{70-80}$) with an IC_{50} of 0.49 μM (pIC_{50} ± S.E. = 6.31 ± 0.04) (Fig. 3*A*), in agreement with its IC_{50} values in the FMP and Ca^{2+}/Fluo-4 assays

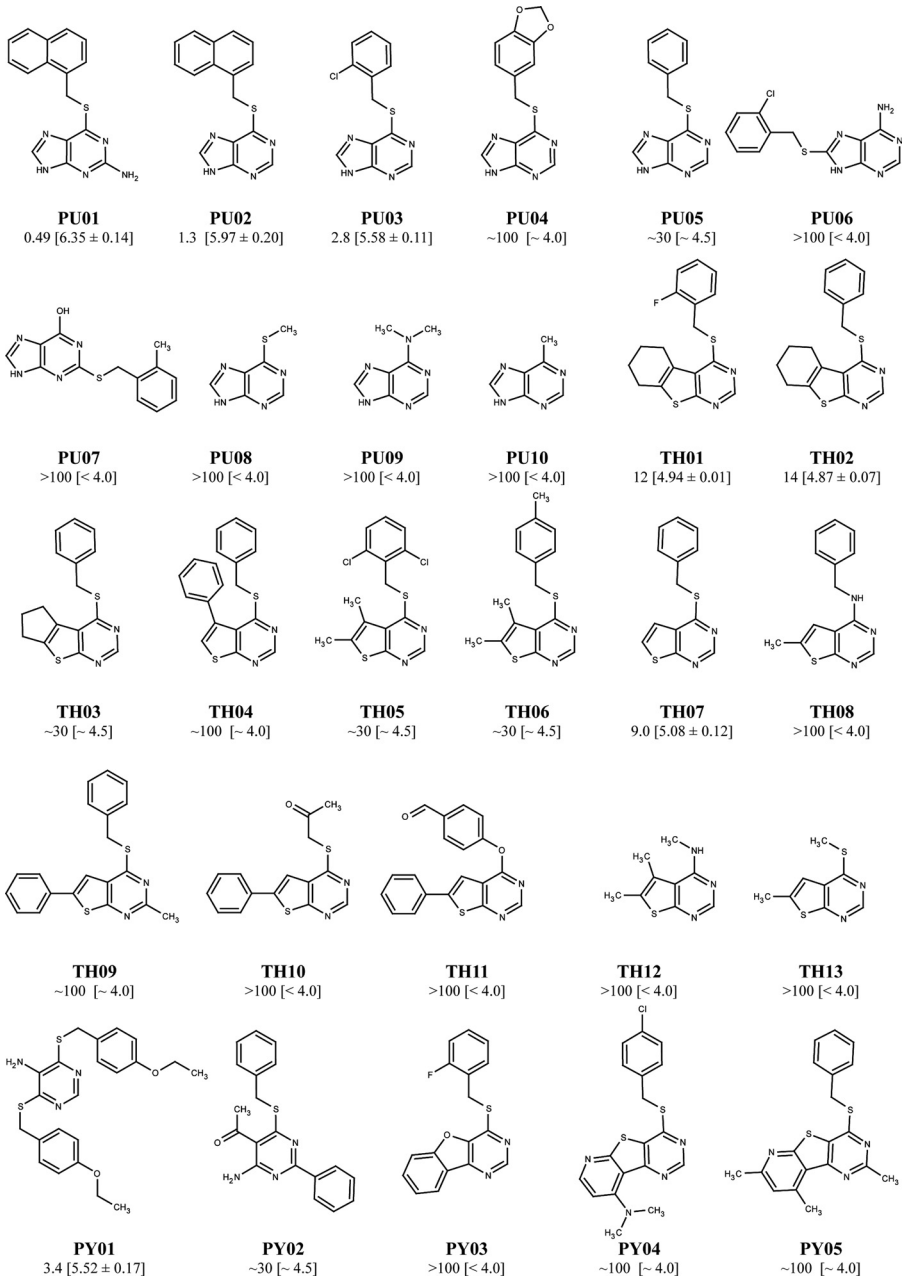

FIGURE 1. **Chemical structures of PU01 and 27 analogs and their respective IC_{50} values (with pIC_{50} ± S. E. values in *brackets*) at the stable h5-HT$_3$A-HEK293 cell line determined in the FMP assay using 5-HT EC_{80} as agonist concentrations.** The prefixes *PU*, *TH*, and *PY* are used for subgroups of compounds in the series containing purine, thienopyrimidine, and pyrimidine ring systems, respectively.

(Fig. 2*A*). As reflected in the current traces (Fig. 3*B*), the τ values obtained for the association and desensitization phases of the 5-HT-mediated response through 5-HT$_3$A in the absence or presence of 0.3 μM PU02 did not differ significantly (Fig. 3*C*).

Mechanism of Action of PU02—In contrast to the competitive 5-HT$_3$R antagonist tropisetron, PU02 did not inhibit the binding of the orthosteric radioligand [^{3}H]GR65630 to the 5-HT$_3$A receptor (IC_{50} >100 μM; Fig. 4*A*). In the FMP assay, the concentration-dependent nature of the PU02 antagonism was demonstrated by determination of 5-HT concentration curves at 5-HT$_3$A in the presence of various concentrations of PU02 (Fig. 4*B*). The impact of pre-exposure of the 5-HT$_3$A receptor to 10 nM ondansetron or 30 μM PU02 (~30-fold higher concentrations than the IC_{50} values) followed by extensive washing on receptor function was also investigated in this assay (Fig. 4*C*). Whereas preincubation with ondansetron did not change 5-HT potency markedly, pre-exposure to PU02 gave rise to a ~10-fold increased 5-HT EC_{50} value, which may be indicative of a slow off-rate of the NAM from the receptor (Fig. 4*C*).

Identification of the PU02 Binding Site and Construction of a 5-HT$_3$A TMD Homology Model—The PU02 binding site in the 5-HT$_3$A receptor was identified through functional characterization of 5-HT, ondansetron, and PU02 at WT and 46 mutant receptors transiently expressed in tsA201 cells in the FMP assay (Figs. 5–7 and Table 2). Originally, the search was based on the hypothesis that PU02 could act through a cavity in the TMD,

which is a common allosteric site in the Cys-loop receptor family and is the site of action for general anesthetics in GlyRs and $GABA_A$Rs (16). Etomidate, a $GABA_A$R PAM, also acts via an intersubunit site in the $\alpha1\beta3$ $GABA_A$R TMD through interactions with Met^{263} in TM1 of $\alpha1$ and Asn^{290} and Met^{311} in TM2 and TM3 of $\beta3$, respectively (Fig. 8) (40, 41). Thus, the first exploratory round of 5-HT$_3$A mutants included Ala mutations of the corresponding Phe^{255}, Leu^{288}, and Val^{310} residues (Fig. 8). While transient expression of the F255A and L288A 5-HT$_3$A mutants in tsA201 cells did not result in the formation of functional receptors in the FMP assay, 5-HT and ondansetron exhibited EC_{50} and IC_{50} values at the V310A mutant similar to those at the WT receptor. In contrast, PU02 displayed a 5-fold higher IC_{50} value at the mutant than at the WT 5-HT$_3$A receptor (Fig. 5 and Table 2).

The modestly impaired PU02 activity arising from the V310A mutation prompted us to explore the putative contributions of Val^{310} and residues in its proximity to PU02 binding. To guide these explorations, a homology model of the human 5-HT$_3$A TMD was constructed. Because the assumed binding site area is located in the subunit interface of the TMD, involving residues from the TM1, TM2, and TM3 helices (16, 40, 41), our homology model comprises a dimer of TM1 to -3, excluding TM4. As a NAM, PU02 is expected to bind to an inactive receptor state, and thus our homology model was constructed based on the crystal structure of the ELIC Cys-loop receptor ortholog from *E. chrysanthemi* (9), the only high resolution x-ray crystal structure of Cys-loop receptor with a closed ion channel available at the time. The *Torpedo* nAChR electron microscopy structure was not regarded as a suitable template due to its low resolution and because it is questionable whether it corresponds to a closed ion channel state (7). Despite ELIC being of prokaryotic origin and showing low amino acid sequence identity to eukaryotic Cys-loop receptors, it is clearly structurally homologous to the *Torpedo* nAChR and other eukaryotic Cys-loop receptors (42), making it a suitable template. To overcome the low sequence identity, a recent NMR structure of the $\beta2$ nAChR (32) was used as a structural link to establish an unequivocal alignment of the amino acid sequence of 5-HT3A to that of ELIC.

In the model, Val^{310} is situated in the third helical turn from the top of TM3, where it lines a predominantly hydrophobic cavity in the subunit interface made up by TM2 and TM3 in the (+)-subunit and TM1 and TM2 in the (−)-subunit (Fig. 9, *A* and *B*). The candidate residues selected for mutagenesis were predominantly those predicted to shape the observed cavity, but residues in the close vicinity of these were also mutated. The residues were initially substituted with amino acids expected to significantly alter their respective interactions with PU02. Residues identified as important for PU02 activity were subsequently subjected to additional mutations to probe the nature of and the spatial requirements for the putative interactions.

Mapping of the PU02 Binding Site—No significant response was observed in tsA201 cells transfected with 18 of the 46 5-HT$_3$A mutants in the FMP assay (5-HT EC_{50} >100 μM; Table 2). The reasons for these lacks of responses were not investigated further. Although the maximal responses elicited by 5-HT through some of the 28 functional mutants differed substantially from that in WT 5-HT$_3$A-expressing cells, the potencies displayed by 5-HT at the vast majority of the mutants did not, as only I290N and L288R displayed EC_{50} values more than

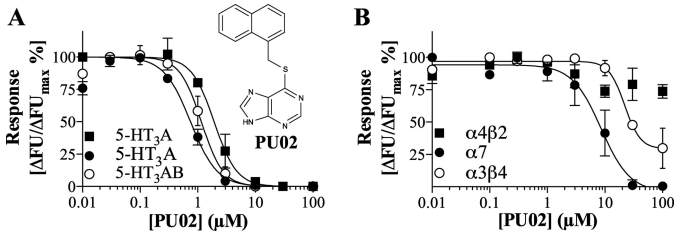

FIGURE 2. **Functional properties of PU02 at 5-HT$_3$Rs and nAChRs.** *A*, chemical structure of PU02 and concentration-inhibition curves for PU02 at human 5-HT$_3$A-HEK293 cells in the FMP assay (■) and at human 5-HT$_3$A- (●) and 5-HT$_3$AB-HEK293 cells (○) in the Ca^{2+}/Fluo-4 assay. *B*, concentration-inhibition curves for PU02 at mouse $\alpha4\beta2$-HEK293T, rat $\alpha3\beta4$-HEK293, and human $\alpha7$-GH3 cells in the FMP ($\alpha4\beta2$, $\alpha3\beta4$) and Ca^{2+}/Fluo-4 ($\alpha7$) assays. The assays were performed as described under "Experimental Procedures," using EC_{80} agonist concentrations, and the results shown represent data ± S.D. (*error bars*) of duplicate determinations from single representative experiments (n = 3–5).

TABLE 1

Functional characteristics of PU02 at 5-HT$_3$Rs and other Cys-loop receptors in the FMP assay or in the Ca^{2+}/Fluo-4 assay

The characterization of PU02 was performed at stable cell lines expressing the receptors or at receptors transiently expressed in tsA201 cell lines. The prefixes "h", "m", and "r" are used for human, mouse, and rat receptors, respectively. The IC_{50} values for PU02 were determined using EC_{70-90} concentrations of agonists for the respective receptors (determined on the day of the experiment) and are given in μM with pIC_{50} ± S.E. values in parentheses. Results are based on 3– 4 individual experiments performed in duplicate as described under "Experimental Procedures."

Receptor	Expression, cell line	Assay	IC_{50} (pIC_{50} ± S.E.)
			μM
5-HT$_3$Rs			
h5-HT$_3$A	Stable, HEK293	FMP	1.3 (5.89 ± 0.20)
h5-HT$_3$A	Stable, HEK293	Ca^{2+}/Fluo-4	0.36 (6.44 ± 0.18)
h5-HT$_3$AB	Stable, HEK293	Ca^{2+}/Fluo-4	0.73 (6.14 ± 0.15)
h5-HT$_3$A	Transient, tsA201	FMP	0.62 (6.21 ± 0.09)
h5-HT$_3$AB	Transient, tsA201	FMP	0.43 (6.37 ± 0.11)
h5-HT$_3$AC	Transient, tsA201	FMP	0.84 (6.08 ± 0.13)
h5-HT$_3$AE	Transient, tsA201	FMP	0.71 (6.15 ± 0.09)
Other Cys-loop receptors			
m$\alpha4\beta2$ nAChR	Stable, HEK293T	FMP	100 (<4)
r$\alpha3\beta4$ nAChR	Stable, HEK293	FMP	~30 (~4.5)
h$\alpha7$ nAChR	Stable, GH3	Ca^{2+}/Fluo-4	9.1 (5.04 ± 0.04)
h$\alpha1$ GlyR	Stable, HEK293	FMP	>100 (<4)
h$\rho1$ $GABA_A$R	Stable, HEK293	FMP	>100 (<4)
h$\alpha1\beta2\gamma2s$ $GABA_A$R	Transient, tsA201	FMP	>100 (<4)

3-fold different from that of WT 5-HT$_3$A (Fig. 5*A* and Table 2). The functional properties of ondansetron and PU02 were determined using EC_{80} (EC_{70}–EC_{90}) 5-HT concentrations for the respective WT and mutant receptors, thus enabling direct comparison of the IC_{50} values. Ondansetron IC_{50} values obtained at the mutants ranged from 0.19 to 2.0 nM and thus were similar to that at WT 5-HT$_3$A (IC_{50} 0.55 nM) (Fig. 5*B* and Table 2). Statistical analysis found 5-HT pEC_{50} and ondansetron pIC_{50} values displayed by some of the mutants to be significantly different from those at the WT receptor (Table 2). However, these differences are not considered pertinent from a biological perspective.

As for PU02, mutations of Phe^{244}, Phe^{255}, Met^{257}, Phe^{287}, Thr^{302}, and Met^{313} in 5-HT$_3$A did not alter its antagonistic activity markedly. However, mutations of Ser^{292} and Val^{310} in the receptor gave rise to subtle increases in PU02 IC_{50}, and mutations of Ser^{248}, Leu^{288}, Ile^{290}, Thr^{294}, and Gly^{306} dramatically altered the functional properties of the antagonist. Whereas PU02 displayed WT-like IC_{50} values at S248A and S292A, the $IC_{50}^{mutant}/IC_{50}^{WT}$ ratios at other mutants ranged from 3–7 (S292Q, V310A, V310L, and V310T) over 12–65 (S248Q, L288M, L288R, I290A, and G306S) to ≥200 (S248N, I290N, and G306I), the latter mutants being virtually insensitive to 100 μM PU02. Interestingly, the effects of the "intermediate group" mutations S248Q, L288M, and G306S were additive, as the three double mutants combining these mutations were completely insensitive to PU02 (Figs. 5*C* and 6 and Table 2).

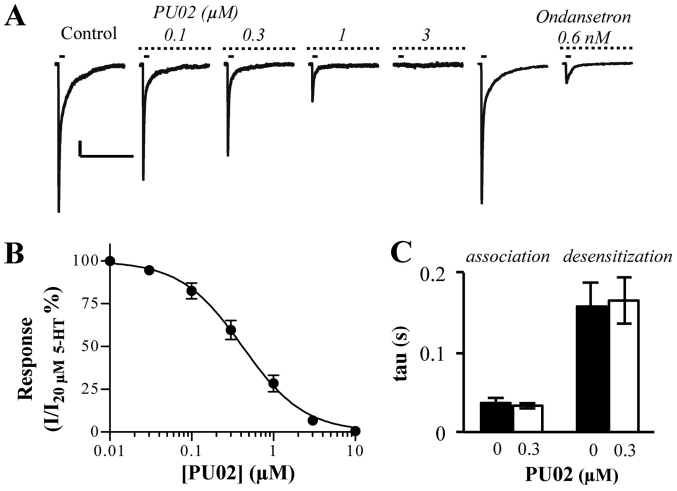

FIGURE 3. **Electrophysiological characterization of PU02 at the 5-HT$_3$A receptor expressed in COS-7 cells.** *A*, currents induced by 20 μM 5-HT (~EC_{70-80}) pulses (*solid bar*, 45-s interval) were inhibited by PU02 (*dotted bar*). *Scale bars*, 200 pA (*vertical*) and 5 s (*horizontal*). Peak current amplitudes induced by 20 μM 5-HT in the presence of PU02 were base line-subtracted and normalized to those in absence of antagonist. *B*, concentration-inhibition curve for PU02. Data are given as mean ± S.E. values (*error bars*) based on 5–6 cells on at least three different days and transfections. *C*, association (current rise) and desensitization (current decay) time constants (τ values) for the 5-HT response in the absence or presence of 0.3 μM PU02 were calculated by fitting either phase of selected currents to applicable single exponential equations.

Mutation-induced Conversion of PU02 into a Complex Allosteric Modulator—Highly interestingly, PU02 exhibited seemingly biphasic concentration-effect curves at the S248V, T294A, T294L, T294Q, and G306A 5-HT$_3$A mutants in the FMP assay, as the responses elicited by EC_{80} 5-HT were potentiated by low and inhibited by high PU02 concentrations (Fig. 6). This dual action style of modulation of these mutants was further investigated by determination of full 5-HT concentration curves in the presence of five PU02 concentrations in the FMP assay (Fig. 7). The results turned out to be quite complex, as can be seen for the S248V mutant. Whereas low PU02 concentrations left-shifted the 5-HT concentration-response relationship at the mutant, high PU02 concentrations caused a right shift (Fig. 7). Notably, at all concentrations of PU02, the maximal response elicited by 5-HT through the S248V mutant was significantly increased (Fig. 7). The profiles displayed by PU02 at the four other mutants were of similar character (Fig. 7).

Electrophysiological Characterization of PU02 at Selected 5-HT$_3$A Receptor Mutants—The detrimental impairment of PU02 activity brought on by introduction of the three mutations S248N, G306I, and L288M/G306S in 5-HT$_3$A was verified in electrophysiological recordings at the mutants expressed in COS-7 cells (Fig. 10). Since the 5-HT EC_{50} values at these mutants are similar to that at WT 5-HT$_3$A, 20 μM 5-HT was used as the agonist concentration for these recordings, just as in the electrophysiological characterization of PU02 at the WT receptor (Fig. 3). The ability of PU02 to inhibit 5-HT-evoked currents through all of these three mutants was dramatically impaired compared with WT 5-HT$_3$A (Fig. 10, *A* and *B*). In contrast, 0.6 nM ondansetron antagonized the 5-HT response through the WT receptor and all three mutants (Figs. 3 and 10*A*). The association and desensitization time constants for

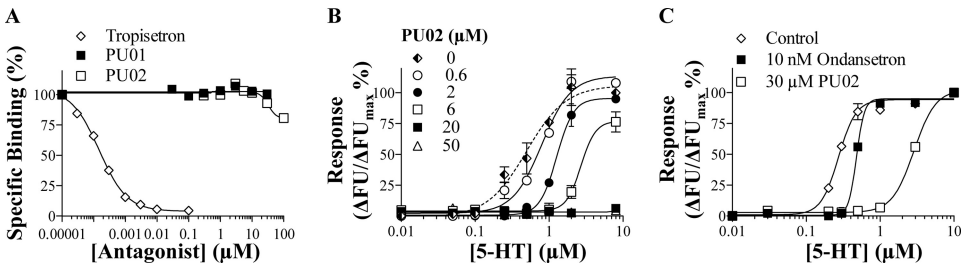

FIGURE 4. **Mechanism of action of PU02 at the human 5-HT$_3$A receptor.** *A*, concentration-inhibition curves for tropisetron, PU01, and PU02 in the [^{3}H]GR65630 competition binding assay to 5-HT$_3$A-HEK293 cell membranes. Tropisetron inhibited [^{3}H]GR65630 binding to the receptor with a pK_i ± S.E. value of 9.59 ± 0.18 (n = 3). *B*, concentration-response curves of 5-HT at 5-HT$_3$A-HEK293 cells in the absence or presence of five different concentrations of PU02 in the FMP assay. No significant response was observed upon application of 5-HT concentrations up to 100 μM when PU02 was present in the assay at concentrations of 20 μM and above (not shown). *C*, concentration-response curves for 5-HT at 5-HT$_3$A-HEK293 cells in the FMP assay after preincubation of the cells with Krebs buffer or with Krebs buffer supplemented with 30 μM PU02 or 10 nM ondansetron for 30 min followed by three rounds of washes with Krebs buffer. The experiments were performed as described under "Experimental Procedures," and the figures depict data ± S.D. (*error bars*) of duplicate determinations from representative experiments (n = 3–4). *FU*, fluorescence units.

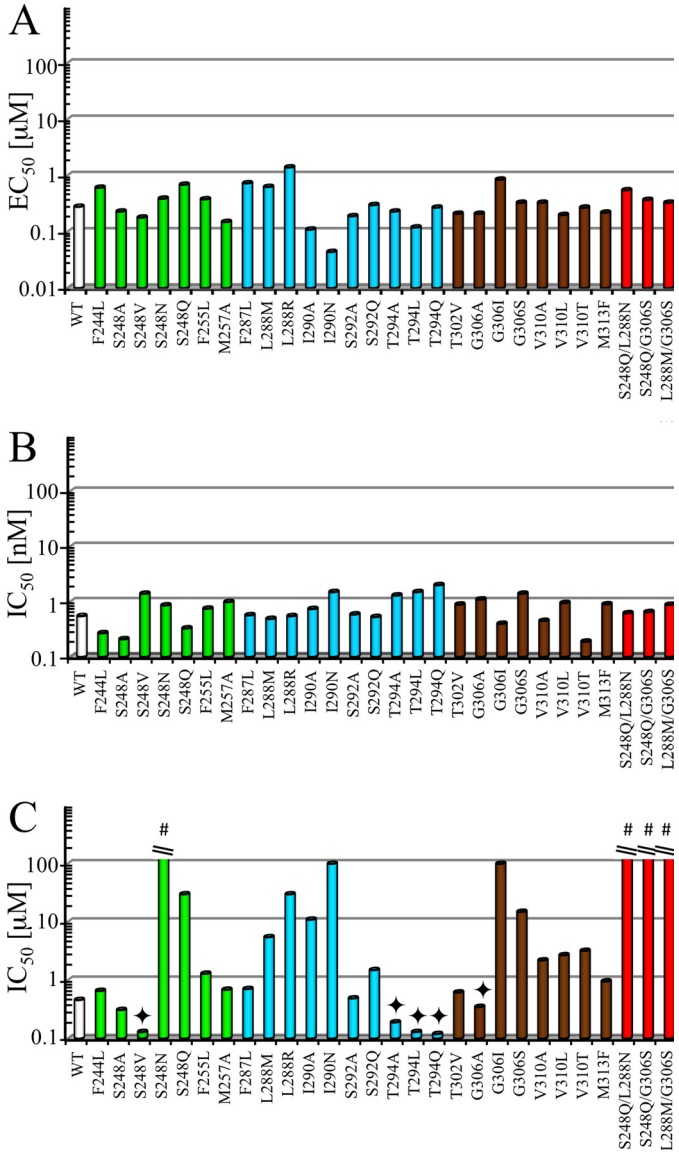

FIGURE 5. **Summation of functional properties of 5-HT, ondansetron and PU02 at the functional 5-HT$_3$A mutants.** EC_{50} values for 5-HT (*A*) and IC_{50} values for ondansetron (*B*) and PU02 (*C*) at WT and functional mutant 5-HT$_3$A receptors transiently expressed in tsA201 cells in the FMP assay. The *bars* for mutants with mutations in TM1, TM2, or TM3 are shown in *green*, *cyan*, and *brown*, respectively, and the *bars* for the three double mutants are shown in *red*. The experiments were performed as described under "Experimental Procedures" using EC_{80} 5-HT concentrations, and detailed data are given in Table 2. #, $IC_{50} > 100$ μM. ♦, complex modulation of PU02. The *bar* represents the EC_{50} for the PAM activity of PU02 at the mutant.

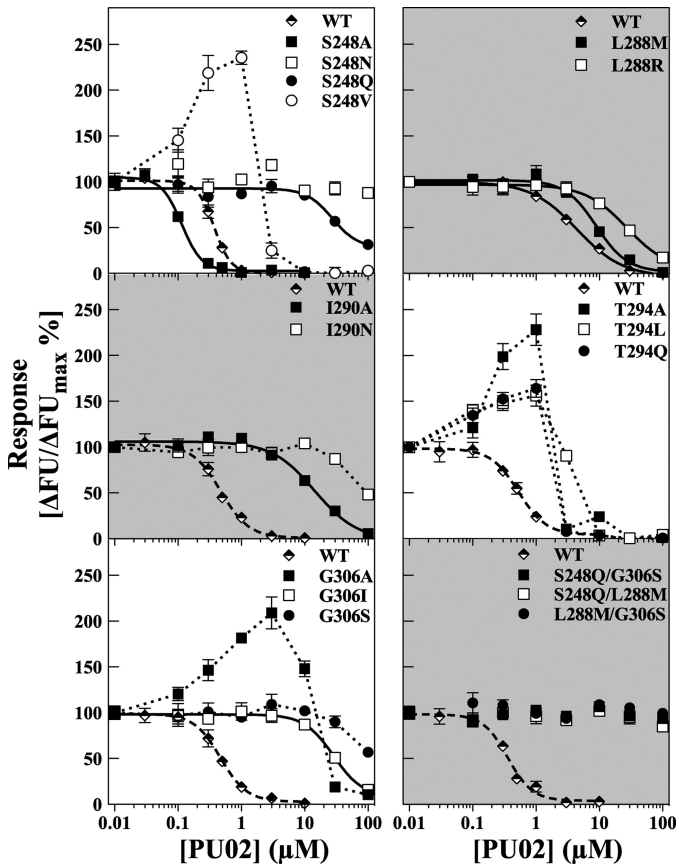

FIGURE 6. **Functional properties of PU02 at WT and selected mutant 5-HT$_3$A receptors in the FMP assay.** The concentration-inhibition curves for PU02 were obtained using EC_{70}–EC_{90} 5-HT concentrations at WT and 5-HT$_3$A mutants containing mutations of the Ser^{248}, Leu^{288}, Ile^{290}, Thr^{294}, or Gly^{306} residue transiently expressed in tsA201 cells. Responses are given as percentage of the 5-HT response in the absence of antagonist. The experiments were performed as described under "Experimental Procedures," and the results shown represent data ± S.D. (*error bars*) of duplicate determinations from single representative experiments ($n = 3$–4). *FU*, fluorescence units.

the mutants did not differ significantly from those of the WT receptor, except for mutant S248N that displayed an increased desensitization time constant (Fig. 10*C*). The presence of 3 μM or 10 μM PU02 during the recordings did not significantly affect any of these parameters (data not shown).

Suggested Binding Mode of PU02 to the 5-HT$_3$A Receptor—Because the 5-HT$_3$A TMD homology model could potentially only include a part of the PU02 binding site, it is not suitable for binding mode prediction by automated molecular docking. However, to insert the experimental results in a structural context, PU02 was manually placed in the hydrophobic cavity in the model (Fig. 9, *C* and *D*), taking all mutagenesis data and the shape of the cavity into consideration. In the model, the seven residues found to be important for PU02 activity are located within the first three upper helix turns in the TMD, where they define a cavity in the subunit interface, the (+)-subunit contributing with Leu^{288} and Ser^{292} (TM2) and Gly^{306} and Val^{310} (TM3) and the (−)-subunit contributing with Ser^{248} (TM1) and Ile^{290} and Thr^{294} (TM2) (Fig. 9). The Leu^{288} and Ile^{290} residues shape the binding cavity and comprise a major part of the total van der Waals interactions with PU02. The 13- and 20-fold increased PU02 IC_{50} values arising from the conservative L288M and I290A mutations, respectively, are in line with loss of van der Waals contacts. Furthermore, the introduction of hydrophilic side chains into the hydrophobic cavity in L288R and I290N would be expected to impair PU02 binding substantially, most likely by repelling the naphthalene moiety of the ligand. The main contribution of Ser^{248} and Gly^{306} to PU02 binding is to define the necessary size of the cavity. Thus, whereas the lack of effect of the S248A mutation shows that Ser^{248} does not form a hydrogen bond to PU02, most substitutions of these two residues introduce a steric clash with the ligand. This is consistent with the detrimental effects on PU02 activity of the larger side chains introduced in S248N, S248Q,

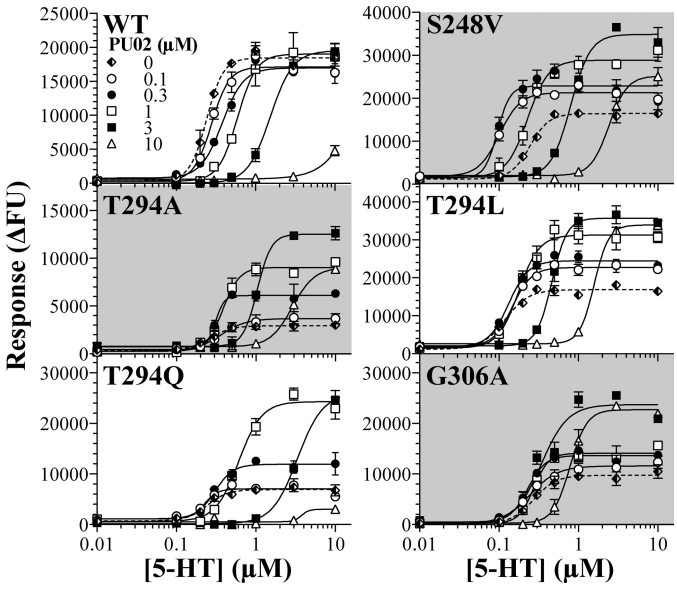

FIGURE 7. **The complex modulation of the signaling of five mutant 5-HT$_3$A receptors exerted by PU02.** Concentration-response curves for 5-HT in the absence or presence of five different concentrations of PU02 at tsA201 cells expressing WT, S248V, T294A, T294L, T294Q, and G306A 5-HT$_3$A receptors in the FMP assay. The experiments were performed as described under "Experimental Procedures," and the results shown represent data ± S.D. (*error bars*) of duplicate determinations from representative experiments (n = 3–4). *FU*, fluorescence units.

G306I, and G306S (Fig. 5 and Table 2). As for Thr^{294}, its hydroxyl group projects into the cavity, where it may form a hydrogen bond with the 7-nitrogen of the purine moiety in PU02 (Fig. 9*C*). The complex profile exhibited by PU02 at mutants with Ala, Leu, or Gln residues in this position certainly underlines its importance for the modulation exerted by PU02 (Fig. 6). Finally, the subtle effects of Ser^{292} and Val^{310} mutations on PU02 activity are consistent with both residues being located in the periphery of the cavity, one helix turn above Leu^{288} and below Gly^{306}, respectively (Fig. 9*C*).

The mutations introduced in 5-HT$_3$A having no impact on PU02 activity can also be rationalized by the homology model, as the residues either are situated in the periphery of the binding site or seem able to adopt side chain conformations pointing away from the ligand (Fig. 9*B*). Interestingly, the Phe^{309} residue is predicted to project directly into the cavity, where it, together with Leu^{288}, defines the bottom of the binding site (Fig. 9*B*). Although it could not be verified experimentally because substitutions of Phe^{309} with several non-aromatic residues yielded non-functional receptors, we propose that Phe^{309} may form π-π interactions with the naphthalene moiety of PU02 and thus could be another important molecular determinant of PU02 binding.

DISCUSSION

PU02 is a novel 5-HT$_3$R antagonist displaying functional IC$_{50}$ values around 1 μM at human 5-HT$_3$Rs, when measured in fluorescence-based assays or by patch clamp electrophysiology and substantially lower potencies at other Cys-loop receptors (Figs. 2*A* and 3*D* and Table 1). The structure of PU02 differs notably from those of orthosteric 5-HT$_3$R ligands, and thus it is hardly surprising that it acts as a NAM, as witnessed by its inability to compete with [^{3}H]GR65630 binding and the complete elimination by 20 μM PU02 of responses evoked by 5-HT concentrations as high as 100 μM (Fig. 4, *A* and *B*). Furthermore, the similar τ values for the association and desensitization of 5-HT-mediated currents through 5-HT$_3$A obtained in the absence and presence of PU02 suggest that the NAM exerts its effects by affecting channel gating efficiency rather than modulating desensitization properties of the receptor (Fig. 3*C*).

Given the structure of PU02, we found it likely that it would target the TMD of the 5-HT$_3$R, analogously to what has been reported for other Cys-loop receptor modulators (12, 40, 41, 43–45). The insights into etomidate binding to GABA$_A$Rs (40, 41) formed the basis for an elaborate mutagenesis study, in which Ser^{248}, Leu^{288}, Ile^{290}, Thr^{294}, and Gly^{306} were identified as important molecular determinants of the PU02 activity at 5-HT$_3$A, and Ser^{292} and Val^{310} were identified as minor contributors (Figs. 5 and 9, *C* and *D*). The fact that all mutants containing substitutions of these residues displayed 5-HT EC$_{50}$ and ondansetron IC$_{50}$ values similar to those at the WT receptor demonstrate that basic receptor function has not been compromised, and thus the observed effect of a given mutation on PU02 potency is largely attributable to its impact on the receptor-NAM interaction. Two potential explanations for the effects of these mutations on PU02 activity come to mind: (i) the mutations could allosterically alter the structural architecture of a distant PU02 binding site, or (ii) the mutated residues could contribute directly to PU02 binding. The substantially decreased inhibitory potencies displayed by PU02 at several of these mutants strongly suggest that the introduced mutations directly impair or disrupt PU02 binding to the 5-HT$_3$A receptor. To our knowledge, cases of mutations allosterically affecting the activity of a ligand acting through a distant site to the degree observed here without also having marked effects on basic receptor function have not been reported. Moreover, in view of the large spectrum of inhibitory potencies and the overall similar maximal NAM efficacies displayed by PU02 at these mutants, it seems highly unlikely that these residues only are "efficacy modulators" of the PU02 activity at the receptor. For instance, the almost complete elimination of PU02 activity arising from single mutations of Ser^{248}, Leu^{288}, Ile^{290}, and Gly^{306} cannot all be ascribed to allosterically mediated changes in a distant binding site. Hence, we conclude that the identified residues line the hydrophobic cavity in the 5-HT$_3$A TMD and directly participate in PU02 binding.

As presented under "Results," our suggested binding mode of PU02 to the 5-HT$_3$A receptor is highly consistent with the mutagenesis data. The predominantly hydrophobic residues making up the intersubunit cavity match the hydrophobic naphthalene moiety of PU02 proposed to bind here. The thioether spacer enables the purine group of PU02 to protrude out of the TMD and form a hydrogen bond to Thr^{294} (Fig. 9, *C* and *D*). Considering its location in the extracellular space, the purine group most likely forms additional bonds with residues in the TM2-TM3 linker and/or the ECD loops L2, L7, and L9 known to be in proximity to the TMD during signal transduction (Fig. 9, *C* and *D*) (5, 14, 15). The suggested binding mode of PU02 is supported by observations from the structure-activity relationship study, where the functional properties of analogs

TABLE 2

Functional characteristics of 5-HT, ondansetron, and PU02 at WT and mutant 5-HT$_3$A receptors transiently expressed in tsA201 cells in the FMP assay

The positions of the mutations in the respective mutants are indicated, the terms (+) and (−) referring to the two subunits forming the intersubunit binding site for PU02. The EC_{50} and R_{max} values for 5-HT at the different receptors are given in μM with pEC_{50} ± S.E. values in parentheses and in percentage of the R_{max} at the WT 5-HT$_3$A receptor, respectively. The IC_{50} values for ondansetron and PU02 are given in nM and μM, respectively, with pIC_{50} ± S.E. values in parentheses. In the antagonist experiments, EC_{70}–EC_{90} concentrations of 5-HT at the respective receptors (determined at the day of the experiment) were used. Results are based on 4–14 individual experiments performed in duplicate as described under "Experimental Procedures." The pEC_{50} values of 5-HT and the pIC_{50} values for ondansetron and PU02 were analyzed by one-way analysis of variance followed by Dunnett's multiple comparisons test, where data from mutants were compared with WT data. Asterisks indicate the significance of difference between compared means (*, $p < 0.05$; **, $p < 0.01$).

		5-HT		Ondansetron	PU02
Receptor	Position of mutation	EC_{50} (pEC_{50} ± S.E.)	R_{max} ± S.E.	IC_{50} (pIC_{50} ± S.E.)	IC_{50} (pIC_{50} ± S.E.)
		μM	% of WT R_{max}	nM	μM
WT		0.28 (6.55 ± 0.02)	100	0.55 (9.26 ± 0.04)	0.46 (6.33 ± 0.05)
F244A	(−)-TM1	>100 (<4)	NR[a]	ND[b]	ND
F244L	(−)-TM1	0.61 (6.21 ± 0.07)**	49 ± 7.4	0.27 (9.57 ± 0.05)	0.66 (6.18 ± 0.11)
S248A	(−)-TM1	0.23 (6.64 ± 0.12)	33 ± 1.4	0.21 (9.67 ± 0.14)*	0.31 (6.50 ± 0.02)
S248V	(−)-TM1	0.18 (6.74 ± 0.09)	56 ± 8.2	1.4 (8.87 ± 0.06)**	Complex modulation
S248N	(−)-TM1	0.39 (6.40 ± 0.04)	130 ± 15	0.86 (9.06 ± 0.09)	>100 (<4)
S248Q	(−)-TM1	0.69 (6.16 ± 0.07)**	64 ± 4.9	0.33 (9.48 ± 0.09)	~30 (~4.5)[c]
S248F	(−)-TM1	>100 (<4)	NR	ND	ND
L249T	(−)-TM1	>100 (<4)	NR	ND	ND
F255A	(−)-TM1	>100 (<4)	NR	ND	ND
F255L	(−)-TM1	0.38 (6.42 ± 0.11)	42 ± 9.1	0.75 (9.12 ± 0.09)	1.3 (5.89 ± 0.04)**
M257A	(−)-TM1	0.15 (6.82 ± 0.20)*	77 ± 12	0.99 (9.00 ± 0.21)	0.69 (6.16 ± 0.11)
F287L	(−)-TM2	0.73 (6.14 ± 0.09)**	79 ± 6.7	0.57 (9.25 ± 0.12)	0.71 (6.15 ± 0.10)
L288A	(+)-TM2	>100 (<4)	NR	ND	ND
L288T	(+)-TM2	>100 (<4)	NR	ND	ND
L288N	(+)-TM2	>100 (<4)	NR	ND	ND
L288M	(+)-TM2	0.63 (6.20 ± 0.06)**	60 ± 8.8	0.49 (9.31 ± 0.11)	5.5 (5.26 ± 0.09)**
L288R	(+)-TM2	1.4 (5.84 ± 0.04)**	33 ± 4.1	0.55 (9.26 ± 0.10)	~30 (~4.5)[c]
L288F	(+)-TM2	>100 (<4)	NR	ND	ND
I290A	(−)-TM2	0.11 (6.97 ± 0.01)**	81 ± 7.1	0.74 (9.13 ± 0.04)	11 (4.96 ± 0.07)**
I290N[d]	(−)-TM2	0.044 (7.35 ± 0.03)**	48 ± 5.9	1.5 (8.83 ± 0.05)**	~100 (~4)[c]
V291M	(+)-TM2	>100 (<4)	NR	ND	ND
V291S	(+)-TM2	>100 (<4)	NR	ND	ND
S292A	(+)-TM2	0.19 (6.73 ± 0.03)	76 ± 5.7	0.59 (9.23 ± 0.07)	0.49 (6.31 ± 0.03)
S292Q	(+)-TM2	0.30 (6.52 ± 0.02)	69 ± 4.6	0.53 (9.27 ± 0.10)	1.5 (5.83 ± 0.06)**
T294A	(−)-TM2	0.23 (6.63 ± 0.07)	33 ± 3.9	1.3 (8.90 ± 0.02)*	Complex Modulation
T294L	(−)-TM2	0.12 (6.92 ± 0.05)**	103 ± 13	1.5 (8.84 ± 0.05)**	Complex Modulation
T294Q	(−)-TM2	0.27 (6.57 ± 0.10)	32 ± 7.1	2.0 (8.71 ± 0.14)**	Complex Modulation
T302L	(+)-TM3	>100 (<4)	NR	ND	ND
T302V	(+)-TM3	0.21 (6.69 ± 0.07)	52 ± 4.8	0.89 (9.05 ± 0.07)	0.62 (6.21 ± 0.09)
I305A	(+)-TM3	>100 (<4)	NR	ND	ND
G306A	(+)-TM3	0.21 (6.68 ± 0.05)	109 ± 11	1.1 (8.96 ± 0.05)	Complex Modulation
G306I	(+)-TM3	0.85 (6.07 ± 0.06)**	126 ± 13	0.40 (9.40 ± 0.10)	~100 (~4.0)[c]
G306S	(+)-TM3	0.33 (6.49 ± 0.06)	181 ± 18	1.4 (8.84 ± 0.10)*	~15 (~4.8)[c]
G306D	(+)-TM3	>100 (<4)	NR	ND	ND
F309L	(+)-TM3	>100 (<4)	NR	ND	ND
F309M	(+)-TM3	>100 (<4)	NR	ND	ND
F309H	(+)-TM3	>100 (<4)	NR	ND	ND
V310A	(+)-TM3	0.33 (6.48 ± 0.11)	66 ± 12	0.45 (9.34 ± 0.07)	2.2 (5.66 ± 0.14)**
V310L	(+)-TM3	0.20 (6.70 ± 0.06)	69 ± 9.2	0.95 (9.02 ± 0.09)	2.7 (5.57 ± 0.02)**
V310T	(+)-TM3	0.27 (6.57 ± 0.04)	72 ± 7.3	0.19 (9.79 ± 0.11)**	3.2 (5.50 ± 0.07)**
V310F	(+)-TM3	>100 (<4)	NR	ND	ND
V310W	(+)-TM3	>100 (<4)	NR	ND	ND
M313F	(+)-TM3	0.22 (6.66 ± 0.09)	140 ± 9.8	0.90 (9.05 ± 0.04)	0.96 (6.02 ± 0.09)*
S248Q/L288M	(−)-TM1/(+)-TM2	0.55 (6.26 ± 0.02)**	42 ± 5.3	0.62 (9.21 ± 0.04)	>100 (<4)
S248Q/G306S	(−)-TM1/(+)-TM3	0.37 (6.43 ± 0.01)**	112 ± 11	0.65 (9.19 ± 0.03)	>100 (<4)
L288M/G306S	(+)-TM2/(+)-TM3	0.33 (6.48 ± 0.04)*	126 ± 14	0.88 (9.06 ± 0.07)**	>100 (<4)

[a] NR, no response.
[b] ND, not determined.
[c] Since a complete concentration-inhibition curve could not be obtained for PU02 at this mutant, the IC_{50} value is an estimate.
[d] tsA201 cells expressing this mutant receptor displayed significantly increased basal levels of fluorescence compared with cells expressing WT or the other 5-HT$_3$A receptor mutants.

PU03, PU08, and TH07 identify the presence of both an aromatic group and a heteroaromatic ring separated by a spacer as important pharmacophore elements of PU02 (Fig. 1).

The seven "PU02-binding residues" identified in 5-HT$_3$A are by no means conserved in other Cys-loop receptors, which would explain the inactivity of the NAM at the majority of receptors in this study (Table 1). We will refrain from explaining the activity of PU02 at $\alpha3\beta4$ and $\alpha7$ nAChRs, but several other ligands exhibit dual $\alpha7$ and 5-HT$_3$ activity (4). The seven residues are not even particularly conserved in the other 5-HT$_3$R subunits, which is interesting considering the equipotent antagonism of PU02 at 5-HT$_3$A, 5-HT$_3$AB, 5-HT$_3$AC, and 5-HT$_3$AE receptors (Fig. 2 and Table 1). Since some of these residues in 5-HT3B actually correspond to mutations of 5-HT3A residues shown to be detrimental to PU02 activity (e.g. L288R and I290N) (Fig. 8), the NAM may not be able to bind to B+/B−, A+/B−, or B−/A+ interfaces. Although the subunit arrangement in 5-HT$_3$AB has been proposed to be B-B-A-B-A (46), recent studies strongly suggest the presence of at least one A+/A− interface in the receptor (47, 48), and thus PU02 could be envisioned to inhibit heteromeric 5-HT$_3$R signaling through binding to this TMD interface. In support of this, PU02 exhibits

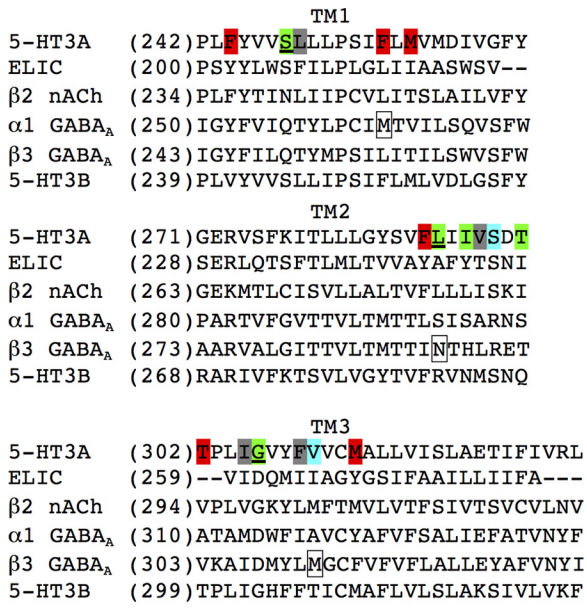

FIGURE 8. **Alignment of amino acid sequences of the TM1, TM2, and TM3 in the human 5-HT3A, ELIC, human β2 nAChR, human α1 GABA$_A$R, human β3 GABA$_A$R, and human 5-HT3B subunits.** The position numbers of the first residue in the respective sequences are shown in *parentheses* to the *left* of the sequences. *Green*, residues in 5-HT3A where at least one of the introduced mutations had a significant effect on PU02 activity. *Cyan*, residues in 5-HT3A where mutations had a weak effect on PU02 activity. *Red*, residues in 5-HT3A where none of the introduced mutations had an effect on PU02 activity. *Gray*, residues in 5-HT3A where all introduced mutations resulted in "non-functional" 5-HT$_3$A receptors. *Underlined*, residues in 5-HT3A where introduced mutations were combined into double mutants. *Boxed*, residues in α1 and β3 GABA$_A$R subunits reported to be important for etomidate activity.

negligible inhibitory activity at the 5-HT$_3$Rs formed in tsA201 cells co-transfected with 5-HT3A-G306I and WT 5-HT3B cDNAs or with 5-HT3A-S248Q and WT 5-HT3B cDNAs in the FMP assay (IC$_{50}$ ~30 μM and ~100 μM, respectively), compared with its IC$_{50}$ of 0.43 μM at WT 5-HT$_3$AB-expressing cells (Table 1) (data not shown).

Our search for the PU02 binding site took its inspiration from that of etomidate (40, 41), and the outcome obviously seems to validate this approach because β3-Asn^{290} and β3-Met^{311} in the GABA$_A$R (40, 41) correspond to Leu^{288} and Val^{310} in the 5-HT$_3$A receptor. However, Val^{310} is located in the periphery of the PU02 site, and α1-Met^{263}, another important determinant of etomidate binding to the GABA$_A$R, aligns with Phe^{255} in 5-HT3A, which is not involved in PU02 binding (Figs. 5 and 9*B*). Thus, although the binding sites for etomidate and PU02 overlap, PU02 seems to target a site in 5-HT$_3$A positioned closer to the extracellular space than etomidate in GABA$_A$Rs. PU02 shares the TMD subunit interface as its site of interaction not only with etomidate but with several other modulators of anionic Cys-loop receptors. Leu^{288} and Val^{310} in 5-HT$_3$A correspond to the Ser^{267} and Ala^{288} residues in α1 GlyR shown to be crucial for the actions of ethanol and general anesthetics (43), and neurosteroids mediate their direct activation of GABA$_A$Rs via binding to an intersubunit site as well (44). Most recently, a crystal structure of the invertebrate glutamate-gated chloride channel GluCl in complex with ivermectin has found this promiscuous allosteric Cys-loop receptor modulator (49, 50) to target this interface as well (13). Ivermectin interacts with residues in (−)-TM1, (+)-TM2, (+)-TM3, and the TM2-TM3 linker in GluCl, several of which correspond to "PU02-binding residues" in 5-HT$_3$A (13). Ivermectin does not protrude as deep into the subunit interface as PU02, however, and thus does not interact with residues in the (−)-TM2 helix (13).

The complex modulation pattern exhibited by PU02 at five 5-HT$_3$A mutants in this study (Figs. 6 and 7) appears to be reminiscent of the profiles of anesthetics at GABA$_A$Rs and GlyRs (51, 52) and of Zn^{2+} at nAChRs and GlyRs (53–56). Biphasic modulation can arise from the existence of distinct high and low affinity sites mediating the potentiation and inhibition of the modulator, respectively, or from the induction of faster receptor desensitization kinetics at higher modulator concentrations (51, 54, 56). We speculate that binding of PU02 to one or a few sites in the mutant receptor could bring about the potentiation observed at low concentrations, whereas occupation of additional sites in the pentamer at higher concentrations could cause the right shift of the 5-HT concentration-response relationship. This is supported by the fact that estimated EC$_{50}$ values for the potentiation exerted by PU02 at these mutants are similar to or lower than its IC$_{50}$ at WT 5-HT$_3$A (Figs. 5*C* and 6). The Thr^{294} residue appears to be a crucial determinant of the nature of PU02 modulation of 5-HT$_3$A because all three mutations of this residue in this study induce the complex modulation pattern (Figs. 6 and 7). More gradual transitions of the PU02 effects are observed for Ser^{248} and Gly^{306}, where the NAM activity at receptors with small residues in these positions (Ser/Ala^{248} and Gly^{306}) is converted into complex modulation of mutants with intermediate size residues (Val^{248} and Ala^{306}) before PU02 becomes inactive at mutants with bigger residues (Asn/Gln^{248} and Ile/Ser^{306}) (Fig. 6). Thus, while PU02 binding affinity may be relatively unaffected by these five mutations, the binding conformation of PU02 in the cavity and/or translation of its binding into effects on channel gating appear to have changed, in agreement with the conclusion that PU02 binding allosterically affects channel activity (Fig. 3*C*).

The recent crystal structures of Cys-loop receptor orthologs have not only confirmed the presence of an intrasubunit and an intersubunit TMD cavity for each of the subunits in the pentameric complex; they have also underlined the tight connection of these to one another via a pore-facing tunnel (9–13). Thus, ligand binding to either of these cavities (12, 13) or the linking tunnel (57) is likely to induce changes in the entire cavity-tunnel system behind the ion pore. The impact on receptor function of ligand binding to these cavities is often acutely sensitive to small changes, be it in receptor or ligand. For example, the NAM and PAM properties of general anesthetics on nAChRs and GABA$_A$Rs/GlyRs, respectively, have been proposed to arise from different shapes and sizes of the intra- and/or intersubunit cavities in the receptors (12). Furthermore, mutations of Met^{253} and Ser^{276} in α7 nAChR, corresponding to Leu^{288} and Val^{310} in 5-HT$_3$A, convert the PAM ivermectin into a NAM (58). This supports the notion that the intersubunit TMD interface not only accommodates the binding of both PAMs and NAMs but that the functional manifestations of ligand binding here are highly fine tuned.

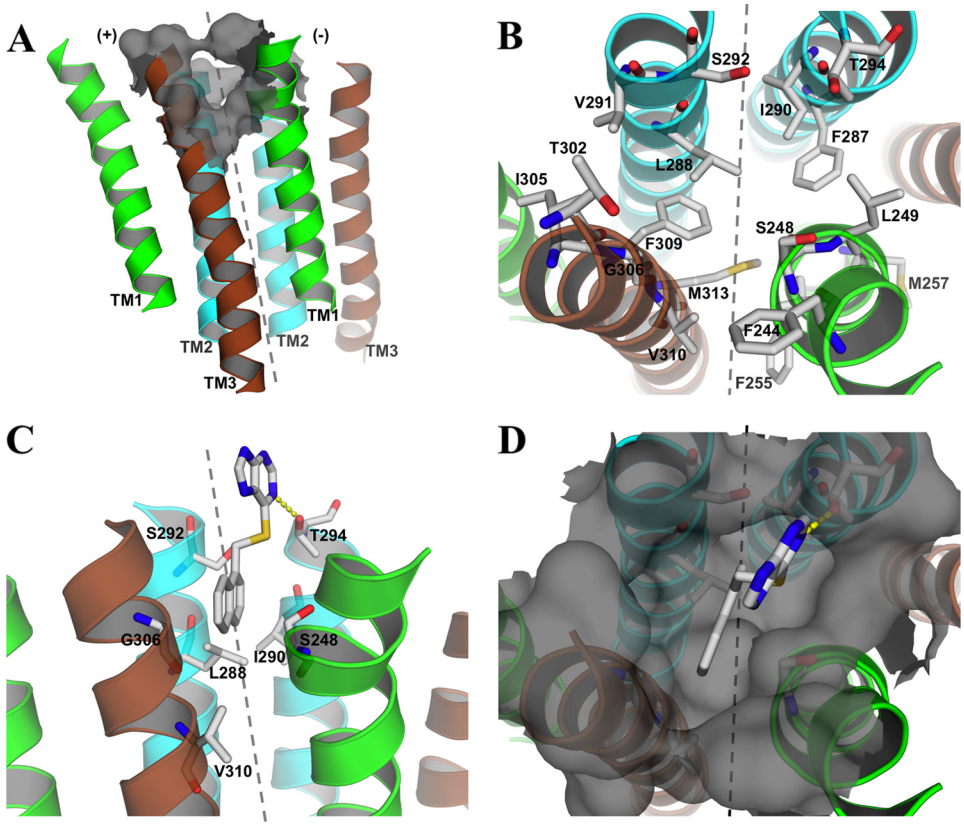

FIGURE 9. **The 5-HT$_3$A TMD dimer homology model.** *A*, complete view of the TM helices TM1 (*green*), TM2 (*cyan*), and TM3 (*brown*) seen from the membrane with the identified cavity represented as a *gray surface*. *B*, top view of the model with stick representations of residues subjected to mutagenesis. *C* and *D*, suggested binding mode of PU02 in 5-HT$_3$A viewed from the membrane (*C*) and from the top (*D*), with a *stick representation* of important residues for PU02 activity. The *dotted gray line* divides the subunit interface into (+)- and (−)-subunits (as denoted in *A*).

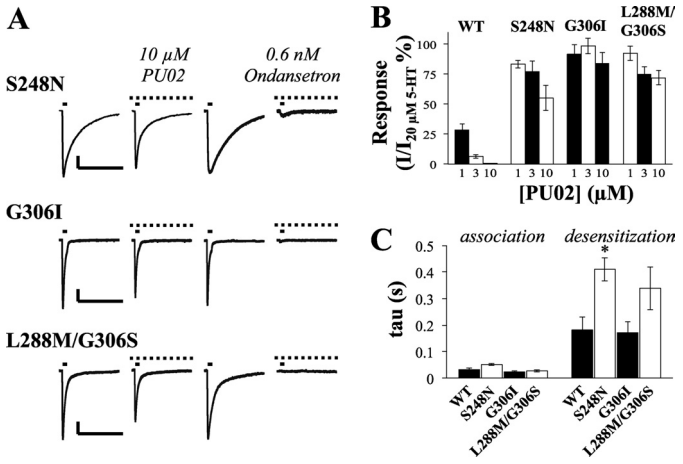

FIGURE 10. **Electrophysiological characterization of PU02 at mutant S248N, G306I, and L288M/G306S 5-HT$_3$A receptors expressed in COS-7 cells.** *A*, currents induced by 20 μM 5-HT pulses (*solid bars*, 45-s interval) in cells expressing S248N, G306I, and L288M/G306S 5-HT$_3$A mutants were not noticeably reduced by 10 μM PU02. *Scale bars*, represent 200 pA (*vertical*) and 5 s (*horizontal*). Peak amplitudes induced by 20 μM 5-HT in the presence of PU02 were base line-subtracted and normalized to those in the absence of antagonist. *B*, summation of the effects of PU02 on WT and mutant 5-HT$_3$A receptor signaling. Data are given as mean ± S.E. values (*error bars*) based on 5–6 cells on at least three different days and transfections. *C*, kinetic parameters of mutants compared with WT receptors. Time constants of association and desensitization for currents evoked by 20 μM 5-HT were calculated as described in the legend to Fig. 3. *Bars*, mean values ± S.E., ($n = 5–7$). Statistical analysis (one-way analysis of variance with a Dunnett's post-test) indicated a significantly (*, $p < 0.05$) increased time constant for the desensitization phase of S248N.

In conclusion, PU02 is the most potent and selective allosteric modulator of 5-HT$_3$Rs reported to date, and to our knowledge, the mapping of the intersubunit binding site for PU02 in the 5-HT$_3$A receptor constitutes one of the most detailed delineations of the molecular basis for an allosteric modulator of a Cys-loop receptor. Moreover, it demonstrates that distantly related bacterial receptor orthologs can be used to construct homology models of these receptors that with high accuracy can predict the location of allosteric sites and the residues comprising these. Finally, the mutation-induced transformation of PU02 from a NAM into a more complex modulator at 5-HT$_3$A bears witness to the subtle structural discrimination between allosteric inhibition and potentiation of this and other Cys-loop receptors and is suggestive of the potential of identifying 5-HT$_3$R PAMs among PU02 analogs.

Acknowledgments—We thank Dr. D. Strøbæk (NeuroSearch A/S) for access to the electrophysiological set-up. We thank Drs. J. Egebjerg, E. F. Kirkness, D. Weiss, P. R. Schofield, P. J. Whiting, C. Rojas, K. Kellar, Y. Xiao, J. A. Stitzel, and D. Feuerbach for generous gifts of cDNAs and cell lines.

REFERENCES

1. Barnes, N. M., Hales, T. G., Lummis, S. C., and Peters, J. A. (2009) The 5-HT$_3$ receptor. The relationship between structure and function. *Neuropharmacology* **56,** 273–284
2. Walstab, J., Rappold, G., and Niesler, B. (2010) 5-HT$_3$ receptors. Role in disease and target of drugs. *Pharmacol. Ther.* **128,** 146–169

3. Jensen, A. A., Davies, P. A., Bräuner-Osborne, H., and Krzywkowski, K. (2008) 3B but which 3B and that's just one of the questions. The heterogeneity of human 5-HT$_3$ receptors. *Trends Pharmacol. Sci.* **29,** 437–444
4. Jensen, A. A., Frølund, B., Liljefors, T., and Krogsgaard-Larsen, P. (2005) Neuronal nicotinic acetylcholine receptors. Structural revelations, target identifications, and therapeutic inspirations. *J. Med. Chem.* **48,** 4705–4745
5. Taly, A., Corringer, P. J., Guedin, D., Lestage, P., and Changeux, J. P. (2009) Nicotinic receptors. Allosteric transitions and therapeutic targets in the nervous system. *Nat. Rev. Drug Discov.* **8,** 733–750
6. Sieghart, W. (2006) Structure, pharmacology, and function of GABA$_A$ receptor subtypes. *Adv. Pharmacol.* **54,** 231–263
7. Unwin, N. (2005) Refined structure of the nicotinic acetylcholine receptor at 4 Å resolution. *J. Mol. Biol.* **346,** 967–989
8. Celie, P. H., van Rossum-Fikkert, S. E., van Dijk, W. J., Brejc, K., Smit, A. B., and Sixma, T. K. (2004) Nicotine and carbamylcholine binding to nicotinic acetylcholine receptors as studied in AChBP crystal structures. *Neuron* **41,** 907–914
9. Hilf, R. J., and Dutzler, R. (2008) X-ray structure of a prokaryotic pentameric ligand-gated ion channel. *Nature* **452,** 375–379
10. Bocquet, N., Nury, H., Baaden, M., Le Poupon, C., Changeux, J. P., Delarue, M., and Corringer, P. J. (2009) X-ray structure of a pentameric ligand-gated ion channel in an apparently open conformation. *Nature* **457,** 111–114
11. Hilf, R. J., and Dutzler, R. (2009) Structure of a potentially open state of a proton-activated pentameric ligand-gated ion channel. *Nature* **457,** 115–118
12. Nury, H., Van Renterghem, C., Weng, Y., Tran, A., Baaden, M., Dufresne, V., Changeux, J. P., Sonner, J. M., Delarue, M., and Corringer, P. J. (2011) X-ray structures of general anesthetics bound to a pentameric ligand-gated ion channel. *Nature* **469,** 428–431
13. Hibbs, R. E., and Gouaux, E. (2011) Principles of activation and permeation in an anion-selective Cys-loop receptor. *Nature* **474,** 54–60
14. Lester, H. A., Dibas, M. I., Dahan, D. S., Leite, J. F., and Dougherty, D. A. (2004) Cys-loop receptors. New twists and turns. *Trends Neurosci.* **27,** 329–336
15. Miller, P. S., and Smart, T. G. (2010) Binding, activation and modulation of Cys-loop receptors. *Trends Pharmacol. Sci.* **31,** 161–174
16. Baenziger, J. E., and Corringer, P. J. (2011) 3D structure and allosteric modulation of the transmembrane domain of pentameric ligand-gated ion channels. *Neuropharmacology* **60,** 116–125
17. Rudolph, U., and Knoflach, F. (2011) Beyond classical benzodiazepines. Novel therapeutic potential of GABA$_A$ receptor subtypes. *Nat. Rev. Drug Discov.* **10,** 685–697
18. Bertrand, D., and Gopalakrishnan, M. (2007) Allosteric modulation of nicotinic acetylcholine receptors. *Biochem. Pharmacol.* **74,** 1155–1163
19. Davies, P. A. (2011) Allosteric modulation of the 5-HT$_3$ receptor. *Curr. Opin. Pharmacol.* **11,** 75–80
20. Rojas, C., Stathis, M., Thomas, A. G., Massuda, E. B., Alt, J., Zhang, J., Rubenstein, E., Sebastiani, S., Cantoreggi, S., Snyder, S. H., and Slusher, B. (2008) Palonosetron exhibits unique molecular interactions with the 5-HT$_3$ receptor. *Anesth. Analg.* **107,** 469–478
21. Xiao, Y., Meyer, E. L., Thompson, J. M., Surin, A., Wroblewski, J., and Kellar, K. J. (1998) Rat α3/β4 subtype of neuronal nicotinic acetylcholine receptor stably expressed in a transfected cell line. Pharmacology of ligand binding and function. *Mol. Pharmacol.* **54,** 322–333
22. Karadsheh, M. S., Shah, M. S., Tang, X., Macdonald, R. L., and Stitzel, J. A. (2004) Functional characterization of mouse α4β2 nicotinic acetylcholine receptors stably expressed in HEK293T cells. *J. Neurochem.* **91,** 1138–1150
23. Feuerbach, D., Lingenhöhl, K., Dobbins, P., Mosbacher, J., Corbett, N., Nozulak, J., and Hoyer, D. (2005) Coupling of human nicotinic acetylcholine receptors alpha 7 to calcium channels in GH3 cells. *Neuropharmacology* **48,** 215–227
24. Jensen, A. A., and Kristiansen, U. (2004) Functional characterization of the human α1 glycine receptor in a fluorescence-based membrane potential assay. *Biochem. Pharmacol.* **67,** 1789–1799
25. Madsen, C., Jensen, A. A., Liljefors, T., Kristiansen, U., Nielsen, B., Hansen, C. P., Larsen, M., Ebert, B., Bang-Andersen, B., Krogsgaard-Larsen, P., and Frølund, B. (2007) 5-Substituted imidazole-4-acetic acid analogues. Synthesis, modeling, and pharmacological characterization of a series of novel γ-aminobutyric acid$_C$ receptor agonists. *J. Med. Chem.* **50,** 4147–4161
26. Krzywkowski, K., Davies, P. A., Feinberg-Zadek, P. L., Bräuner-Osborne, H., and Jensen, A. A. (2008) High-frequency HTR3B variant associated with major depression dramatically augments the signaling of the human 5-HT$_3$AB receptor. *Proc. Natl. Acad. Sci. U.S.A.* **105,** 722–727
27. Krzywkowski, K., Jensen, A. A., Connolly, C. N., and Bräuner-Osborne, H. (2007) Naturally occurring variations in the human 5-HT3A gene profoundly impact 5-HT$_3$ receptor function and expression. *Pharmacogenet. Genomics* **17,** 255–266
28. Jørgensen, C. G., Frølund, B., Kehler, J., and Jensen, A. A. (2011) Discovery of benzamide analogues as a novel class of 5-HT$_3$ receptor agonists. *ChemMedChem* **6,** 725–736
29. Jensen, A. A., Zlotos, D. P., and Liljefors, T. (2007) Pharmacological characteristics and binding modes of caracurine V analogues and related compounds at the neuronal α7 nicotinic acetylcholine receptor. *J. Med. Chem.* **50,** 4616–4629
30. Hamill, O. P., Marty, A., Neher, E., Sakmann, B., and Sigworth, F. J. (1981) Improved patch-clamp techniques for high-resolution current recording from cells and cell-free membrane patches. *Pflugers Arch.* **391,** 85–100
31. Christensen, J. K., Varming, T., Ahring, P. K., Jørgensen, T. D., and Nielsen, E. Ø. (2004) *In vitro* characterization of 5-carboxyl-2,4-di-benzamidobenzoic acid (NS3763), a noncompetitive antagonist of GLUK5 receptors. *J. Pharmacol. Exp. Ther.* **309,** 1003–1010
32. Bondarenko, V., Tillman, T., Xu, Y., and Tang, P. (2010) NMR structure of the transmembrane domain of the *n*-acetylcholine receptor β2 subunit. *Biochim. Biophys. Acta* **1798,** 1608–1614
33. Berman, H. M., Westbrook, J., Feng, Z., Gilliland, G., Bhat, T. N., Weissig, H., Shindyalov, I. N., and Bourne, P. E. (2000) The Protein Data Bank. *Nucleic Acids Res.* **28,** 235–242
34. Notredame, C., Higgins, D. G., and Heringa, J. (2000) T-Coffee. A novel method for fast and accurate multiple sequence alignment. *J. Mol. Biol.* **302,** 205–217
35. DeLano, W. L. (2002) *The PyMOL Molecular Graphics System*, Version 1.4, Schrodinger, LLC
36. UniProt Consortium (2011) Ongoing and future developments at the Universal Protein Resource. *Nucleic Acids Res.* **39,** D214–D219
37. Sali, A., and Blundell, T. L. (1993) Comparative protein modeling by satisfaction of spatial restraints. *J. Mol. Biol.* **234,** 779–815
38. Shen, M. Y., and Sali, A. (2006) Statistical potential for assessment and prediction of protein structures. *Protein Sci.* **15,** 2507–2524
39. Barann, M., Meder, W., Dorner, Z., Brüss, M., Bönisch, H., Göthert, M., and Urban, B. W. (2000) Recombinant human 5-HT$_{3A}$ receptors in outside-out patches of HEK 293 cells. Basic properties and barbiturate effects. *Naunyn Schmiedebergs Arch. Pharmacol.* **362,** 255–265
40. Li, G. D., Chiara, D. C., Sawyer, G. W., Husain, S. S., Olsen, R. W., and Cohen, J. B. (2006) Identification of a GABA$_A$ receptor anesthetic binding site at subunit interfaces by photolabeling with an etomidate analog. *J. Neurosci.* **26,** 11599–11605
41. Belelli, D., Lambert, J. J., Peters, J. A., Wafford, K., and Whiting, P. J. (1997) The interaction of the general anesthetic etomidate with the γ-aminobutyric acid type A receptor is influenced by a single amino acid. *Proc. Natl. Acad. Sci. U.S.A.* **94,** 11031–11036
42. Corringer, P. J., Baaden, M., Bocquet, N., Delarue, M., Dufresne, V., Nury, H., Prevost, M., and Van Renterghem, C. (2010) Atomic structure and dynamics of pentameric ligand-gated ion channels. New insight from bacterial homologues. *J. Physiol.* **588,** 565–572
43. Mihic, S. J., Ye, Q., Wick, M. J., Koltchine, V. V., Krasowski, M. D., Finn, S. E., Mascia, M. P., Valenzuela, C. F., Hanson, K. K., Greenblatt, E. P., Harris, R. A., and Harrison, N. L. (1997) Sites of alcohol and volatile anaesthetic action on GABA$_A$ and glycine receptors. *Nature* **389,** 385–389
44. Hosie, A. M., Wilkins, M. E., da Silva, H. M., and Smart, T. G. (2006) Endogenous neurosteroids regulate GABA$_A$ receptors through two discrete transmembrane sites. *Nature* **444,** 486–489
45. Young, G. T., Zwart, R., Walker, A. S., Sher, E., and Millar, N. S. (2008) Potentiation of α7 nicotinic acetylcholine receptors via an allosteric trans-

membrane site. *Proc. Natl. Acad. Sci. U.S.A.* **105,** 14686–14691
46. Barrera, N. P., Herbert, P., Henderson, R. M., Martin, I. L., and Edwardson, J. M. (2005) Atomic force microscopy reveals the stoichiometry and subunit arrangement of 5-HT$_3$ receptors. *Proc. Natl. Acad. Sci. U.S.A.* **102,** 12595–12600
47. Lochner, M., and Lummis, S. C. (2010) Agonists and antagonists bind to an A-A interface in the heteromeric 5-HT$_3$AB receptor. *Biophys. J.* **98,** 1494–1502
48. Thompson, A. J., Price, K. L., and Lummis, S. C. (2011) Cysteine modification reveals which subunits form the ligand binding site in human heteromeric 5-HT$_3$AB receptors. *J. Physiol.* **589,** 4243–4257
49. Krause, R. M., Buisson, B., Bertrand, S., Corringer, P. J., Galzi, J. L., Changeux, J. P., and Bertrand, D. (1998) Ivermectin. A positive allosteric effector of the α7 neuronal nicotinic acetylcholine receptor. *Mol. Pharmacol.* **53,** 283–294
50. Shan, Q., Haddrill, J. L., and Lynch, J. W. (2001) Ivermectin, an unconventional agonist of the glycine receptor chloride channel. *J. Biol. Chem.* **276,** 12556–12564
51. Adodra, S., and Hales, T. G. (1995) Potentiation, activation, and blockade of GABA$_A$ receptors of clonal murine hypothalamic GT1–7 neurons by propofol. *Br. J. Pharmacol.* **115,** 953–960
52. Pistis, M., Belelli, D., Peters, J. A., and Lambert, J. J. (1997) The interaction of general anaesthetics with recombinant GABA$_A$ and glycine receptors expressed in *Xenopus laevis* oocytes. A comparative study. *Br. J. Pharmacol.* **122,** 1707–1719
53. Hsiao, B., Dweck, D., and Luetje, C. W. (2001) Subunit-dependent modulation of neuronal nicotinic receptors by zinc. *J. Neurosci.* **21,** 1848–1856
54. Hsiao, B., Mihalak, K. B., Repicky, S. E., Everhart, D., Mederos, A. H., Malhotra, A., and Luetje, C. W. (2006) Determinants of zinc potentiation on the α4 subunit of neuronal nicotinic receptors. *Mol. Pharmacol.* **69,** 27–36
55. Bloomenthal, A. B., Goldwater, E., Pritchett, D. B., and Harrison, N. L. (1994) Biphasic modulation of the strychnine-sensitive glycine receptor by Zn^{2+}. *Mol. Pharmacol.* **46,** 1156–1159
56. Miller, P. S., Topf, M., and Smart, T. G. (2008) Mapping a molecular link between allosteric inhibition and activation of the glycine receptor. *Nat. Struct. Mol. Biol.* **15,** 1084–1093
57. Howard, R. J., Murail, S., Ondricek, K. E., Corringer, P. J., Lindahl, E., Trudell, J. R., and Harris, R. A. (2011) Structural basis for alcohol modulation of a pentameric ligand-gated ion channel. *Proc. Natl. Acad. Sci. U.S.A.* **108,** 12149–12154
58. Collins, T., and Millar, N. S. (2010) Nicotinic acetylcholine receptor transmembrane mutations convert ivermectin from a positive to a negative allosteric modulator. *Mol. Pharmacol.* **78,** 198–204